Electronic coherence dynamics in trans-polyacetylene oligomers

Ignacio Franco and Paul Brumer

Citation: J. Chem. Phys. **136**, 144501 (2012); doi: 10.1063/1.3700445
View online: http://dx.doi.org/10.1063/1.3700445
View Table of Contents: http://jcp.aip.org/resource/1/JCPSA6/v136/i14
Published by the American Institute of Physics.

Electronic coherence dynamics in *trans*-polyacetylene oligomers

Ignacio Franco[1,a)] and Paul Brumer[2,b)]
[1]*Department of Chemistry, Northwestern University, Evanston, Illinois 60208-3113, USA*
[2]*Chemical Physics Theory Group and Department of Chemistry, University of Toronto, Toronto, Ontario M5S 3H6, Canada*

(Received 28 November 2011; accepted 19 March 2012; published online 9 April 2012)

Electronic coherence dynamics in *trans*-polyacetylene oligomers are considered by explicitly computing the time dependent molecular polarization from the coupled dynamics of electronic and vibrational degrees of freedom in a mean-field mixed quantum-classical approximation. The oligomers are described by the Su-Schrieffer-Heeger Hamiltonian and the effect of decoherence is incorporated by propagating an ensemble of quantum-classical trajectories with initial conditions obtained by sampling the Wigner distribution of the nuclear degrees of freedom. The electronic coherence of superpositions between the ground and excited and between pairs of excited states is examined for chains of different length, and the dynamics is discussed in terms of the nuclear overlap function that appears in the off-diagonal elements of the electronic reduced density matrix. For long oligomers the loss of coherence occurs in tens of femtoseconds. This time scale is determined by the decay of population into other electronic states through vibronic interactions, and is relatively insensitive to the type and class of superposition considered. By contrast, for smaller oligomers the decoherence time scale depends strongly on the initially selected superposition, with superpositions that can decay as fast as 50 fs and as slow as 250 fs. The long-lived superpositions are such that little population is transferred to other electronic states and for which the vibronic dynamics is relatively harmonic.
 [http://dx.doi.org/10.1063/1.3700445]

I. INTRODUCTION

Electronic decoherence (the decay of the off-diagonal elements of the electronic reduced density matrix) in molecules is a basic feature of the electron-vibrational evolution that accompanies photoexcitation,[1] passage through conical intersections,[2] energy transfer,[3] or any other dynamical process that creates electronic superposition states. In the decoherence language,[4] the electrons are the system of interest, the nuclei act as the bath, and it is the system-bath interaction what leads to the decoherence. Establishing mechanisms for electronic decoherence is central to our understanding of the dynamics underlying fundamental processes such as photosynthesis, vision or electron transport.[2,3,5] It is also vital in the development of approximation schemes to the full vibronic evolution of molecules,[6,7] and it is the starting point for the design of methods to preserve the coherence of electronic superpositions in molecules that can be subsequently exploited in intriguing and potentially useful ways via quantum control[8] or quantum information[9] schemes.

Time scales for electronic decoherence in polyatomic molecules are often exceedingly fast, on the order of tens of femtoseconds.[1,10–12] This time scale is normally determined by the vibrational degrees of freedom of the nuclear dynamics, with slower torsional, rotational, or possible solvent dynamics (if present) playing a secondary role.[10] However, challenges in understanding electronic decoherence have arisen from recent spectroscopic observations that have demonstrated that in some photosynthetic systems electronic coherences can be long-lived,[13–15] with lifetimes exceeding 400–600 fs. These results have lead to discussions of the role of quantum coherences in biological processes and reconsideration of our understanding of decoherence dynamics in single molecules and molecular aggregates.[3,13–24] Many of the associated computations utilize phenomenological models or master equations[25] that approximate the dynamical effects of the bath on the system coordinates without explicitly following the bath dynamics. In these approaches, the effect of the bath on the dynamics is typically determined by adjustable parameters that can be chosen to reproduce experimental findings, when available. When possible, however, explicitly following the dynamics of the nuclei is much preferred.[26,27] This is because electronic decoherence in molecules can be understood as arising from nuclear dynamics on several electronic potential energy surfaces.[1,10–12] For example, for an entangled vibronic state of two levels, of the form

$$|\Psi(t)\rangle = |\phi_i\rangle|\chi_i(t)\rangle + |\phi_j\rangle|\chi_j(t)\rangle \quad (i \neq j), \tag{1}$$

where the $|\phi_n\rangle$ are orthonormal electronic states and $|\chi_n(t)\rangle$ denotes the nuclear state in the nth electronic surface, the electronic reduced density matrix ρ_e is given by

$$\begin{aligned}\rho_e(t) &= \mathrm{Tr_N}\{|\Psi(t)\rangle\langle\Psi(t)|\} \\ &= |\phi_i\rangle\langle\phi_i|\langle\chi_i(t)|\chi_i(t)\rangle + |\phi_j\rangle\langle\phi_j|\langle\chi_j(t)|\chi_j(t)\rangle \\ &\quad +[|\phi_i\rangle\langle\phi_j|\langle\chi_j(t)|\chi_i(t)\rangle + \mathrm{H.c.}].\end{aligned} \tag{2}$$

Here the trace is over the nuclear states and H.c. denotes the Hermitian conjugate. Hence, the decay of the off-diagonal

a)Present address: Theory Department, Fritz Haber Institute of the Max Planck Society, Faradayweg 4-6, 14195 Berlin, Germany. Electronic mail: franco@fhi-berlin.mpg.de.
b)Electronic mail: pbrumer@chem.utoronto.ca.

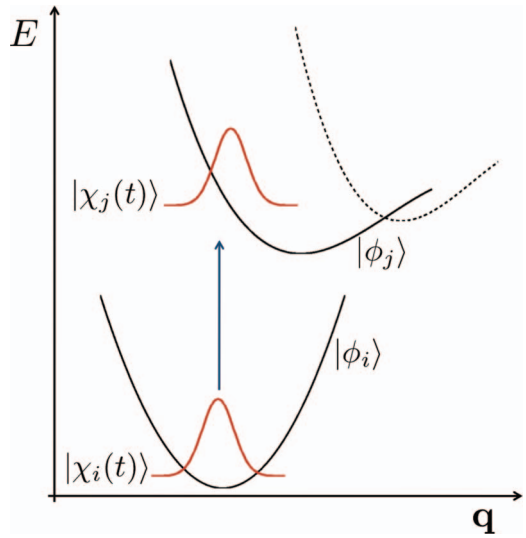

FIG. 1. Evolution and decay of the overlap of the nuclear wavefunctions in two electronic potential energy surfaces $S_{ij}(t) = \langle\chi_j(t)|\chi_i(t)\rangle$ upon instantaneous excitation from state $|\phi_i\rangle$ to state $|\phi_j\rangle$. Both anharmonicities and population transfer to other electronic states (dotted lines) can lead to a decay of $S_{ij}(t)$ and thus to decoherences between $|\phi_i\rangle$ and $|\phi_j\rangle$. In the scheme, E is the energy and $\mathbf{q}$ denotes the general nuclear conformational space.

matrix elements in $\rho_e(t)$, i.e., electronic decoherence, is governed by the degree of overlap of the nuclear wavepackets $S_{ij}(t) = \langle\chi_j(t)|\chi_i(t)\rangle$ associated with the electronic states in the superposition. Thus, by understanding the events that lead to a decay of the overlaps $S_{ij}(t)$ one obtains direct insights into the mechanism of electronic decoherence between states i and j. A schematic representation of such evolution and decay for a particular pair of states is shown in Fig. 1.

In this paper, we present a study of the electronic coherence dynamics in *trans*-polyacetylene (PA) oligomers in which the dynamics of both electronic and vibrational degrees of freedom are explicitly taken into account. We do so in an approximate scheme where the nuclei are considered classically and the electrons quantum mechanically. The oligomers are described using the well-known Su-Schrieffer-Heeger (SSH) Hamiltonian.[28] The SSH model treats the molecule as a tight-binding chain in which the electrons are coupled to distortions in the polymer backbone by electron-vibrational interactions. In spite of its simplicity, the SSH Hamiltonian is remarkably successful in capturing the electronic structure of PA, its photoinduced vibronic dynamics and the rich photophysics of polarons, breathers and kinks.[1,29–31] This model is often used to study the dynamical features caused by strong electron-ion couplings.[1,32,33]

The coupled dynamics of nuclear and electronic degrees of freedom of the molecule is followed in a mean-field (Ehrenfest) mixed quantum-classical approximation[34–36] and decoherence effects are incorporated by propagating an ensemble of quantum-classical trajectories with initial conditions selected from the nuclear Wigner distribution function[1,37–39] of the chain. In this way the dynamics reflects the initial nuclear quantum distribution and is subject to the level broadening and internal relaxation mechanism induced by the vibronic couplings. Using this model we study the possible effect of system size, nuclear initial conditions, and type of electronic superposition states on the dynamics of electronic coherence.

II. MODEL AND METHODS

A. The SSH Hamiltonian

The SSH Hamiltonian[28] models PA oligomers as one-dimensional tight-binding chains, each site representing a CH unit. The Hamiltonian for an N-membered oligomer is given by

$$H_{\rm SSH} = H_{\rm elec} + H_{\rm ph}, \tag{3}$$

where

$$H_{\rm elec} = \sum_{n=1}^{N-1}\sum_{s=\pm1}[-t_0 + \alpha(u_{n+1} - u_n)] \times (c^\dagger_{n+1,s}c_{n,s} + c^\dagger_{n,s}c_{n+1,s}) \quad \text{and,}$$
$$H_{\rm ph} = \sum_{n=1}^{N}\frac{p_n^2}{2M} + \frac{K}{2}\sum_{n=1}^{N-1}(u_{n+1} - u_n)^2, \tag{4}$$

are, respectively, the electronic and nuclear parts of the Hamiltonian. Here, u_n denotes the displacement of the nth CH site from the perfectly periodic position $x = na$ with a as the lattice constant, M is the mass of the CH group, p_n is the momentum conjugate to u_n and K is an effective spring constant. The operator $c^\dagger_{n,s}$ (or $c_{n,s}$) creates (or annihilates) a fermion on site n with spin s and satisfies the usual fermionic anticommutation relations. The electronic component of the Hamiltonian consists of a term describing the hopping of π electrons along the chain with hopping integral t_0 and an electron-ion interaction term with coupling constant α. The quantity α couples the electronic states to the molecular geometry and constitutes a first-order correction to the lowest order hopping integral t_0. Throughout this work, we use the standard set of SSH parameters for PA: $t_0 = 2.5$ eV, $\alpha = 4.1$ eV/Å, $K = 21$ eV/Å^2, $M = 1349.14$ eV fs^2/Å^2, and $a = 1.22$ Å.

B. Ehrenfest electron-vibrational dynamics

The electron-vibrational dynamics of the chain is followed in the mean-field Ehrenfest mixed quantum-classical approximation.[1,35–38] In this approximation, the nuclei move classically on a mean-field potential energy surface with forces given by

$$\dot{p}_n = -\langle\varphi(t)|\frac{\partial H_{\rm SSH}}{\partial u_n}|\varphi(t)\rangle. \tag{5}$$

In turn, the antisymmetrized $\mathcal{N}$ electron wavefunction $|\varphi(t)\rangle$ satisfies the time-dependent Schrödinger equation

$$i\hbar\frac{\partial}{\partial t}|\varphi(t)\rangle = H_{\rm SSH}[\boldsymbol{u}(t)]|\varphi(t)\rangle, \tag{6}$$

where $\boldsymbol{u} \equiv (u_1, u_2, \ldots, u_N)$. Since $H_{\rm SSH}$ is a single-particle operator, the electronic properties of the system are completely characterized by the single-particle electronic

density matrix

$$\rho_{n,m}(t) = \sum_s \langle \varphi(t)|c^\dagger_{n,s}c_{m,s}|\varphi(t)\rangle. \tag{7}$$

From Eq. (6) it follows that the dynamics of $\rho_{n,m}$ satisfies

$$\begin{aligned} i\hbar\frac{\mathrm{d}}{\mathrm{d}t}\rho_{n,m}(t) &= \sum_s \langle \varphi(t)|[c^\dagger_{n,s}c_{m,s}, H_{\mathrm{elec}}]|\varphi(t)\rangle \\ &= \sum_{m'}(h_{m,m'}\rho_{n,m'}(t) - h_{m',n}\rho_{m',m}(t)), \end{aligned} \tag{8}$$

where $h_{n,m} = \langle n, s|H_{\mathrm{elec}}|m, s\rangle$ are the single-particle matrix elements of H_{elec} and $|n, s\rangle = c^\dagger_{n,s}|0\rangle$ where $|0\rangle$ is the vacuum state.

Equation (8) is integrated by decomposing $\rho_{n,m}(t)$ into orbitals. For this, let $|\epsilon,s\rangle$ be the eigenorbitals of spin s and energy ϵ of the system at preparation time ($H_{\mathrm{elec}}(t=0)|\epsilon, s\rangle = \epsilon|\epsilon, s\rangle$). Using this basis, the initial electronic reduced density matrix can be expressed as

$$\rho_{n,m}(0) = \sum_{\epsilon,\epsilon'=1}^{N}\sum_s \langle \epsilon, s|n, s\rangle\langle m, s|\epsilon', s\rangle\langle\varphi(0)|c^\dagger_{\epsilon,s}c_{\epsilon',s}|\varphi(0)\rangle, \tag{9}$$

where $\langle\varphi(0)|c^\dagger_{\epsilon,s}c_{\epsilon',s}|\varphi(0)\rangle$ characterizes the initial electronic distribution among the single particle states, and $|\epsilon, s\rangle = c^\dagger_{\epsilon,s}|0\rangle$. In writing Eq. (9) we have employed the basis transformation function $c^\dagger_{n,s} = \sum_{\epsilon=1}^{N}\langle\epsilon, s|n, s\rangle c^\dagger_{\epsilon,s}$. We adopt the ansatz that upon time evolution $\rho_{n,m}(t)$ maintains the form in Eq. (9). That is,

$$\begin{aligned} \rho_{n,m}(t) = \sum_{\epsilon,\epsilon'=1}^{N}\sum_s &\langle\epsilon(t), s|n, s\rangle\langle m, s|\epsilon'(t), s\rangle \\ &\times\langle\varphi(0)|c^\dagger_{\epsilon,s}c_{\epsilon',s}|\varphi(0)\rangle. \end{aligned} \tag{10}$$

The utility of this ansatz is that if the time-dependent orbitals $|\epsilon(t), s\rangle$ satisfy the single-particle Schrödinger equation

$$i\hbar\frac{\mathrm{d}}{\mathrm{d}t}|\epsilon(t), s\rangle = H_{\mathrm{elec}}(t)|\epsilon(t), s\rangle, \tag{11}$$

with initial conditions $|\epsilon(t=0), s\rangle = |\epsilon, s\rangle$, the reduced density matrix automatically satisfies the correct equation of motion [Eq. (8)].

Within this framework, the equations for the nuclear trajectories are

$$\begin{aligned} \dot{u}_n(t) &= \frac{p_n(t)}{M}; \\ \dot{p}_n(t) &= -K(2u_n(t) - u_{n+1}(t) - u_{n-1}(t)) \\ &\quad + 2\alpha\mathrm{Re}\{\rho_{n,n+1}(t) - \rho_{n,n-1}(t)\}. \end{aligned} \tag{12}$$

The chain is taken to be clamped so that $u_1(t) = u_N(t) = 0$ and $p_1(t) = p_N(t) = 0$ for all time, and Eq. (12) is valid for $n = 2, \ldots, N-1$. In turn, the orbitals that form $\rho_{nm}(t)$ satisfy Eq. (11), so that

$$\begin{aligned} i\hbar\frac{\mathrm{d}}{\mathrm{d}t}\langle n|\epsilon(t)\rangle &= [-t_0 + \alpha(u_{n+1}(t) - u_n(t))]\langle n+1|\epsilon(t)\rangle \\ &\quad + [-t_0 + \alpha(u_n(t) - u_{n-1}(t))]\langle n-1|\epsilon(t)\rangle \end{aligned} \tag{13}$$

for $n, \epsilon = 1, \ldots, N$. Since the electrons are confined within the chain, $\langle n|\epsilon(t)\rangle = 0$ for $n \notin \{1, \ldots, N\}$. Equations (12) and (13) constitute a closed set of $N(N+2)$ coupled first-order differential equations that are integrated using an eighth-order Runge-Kutta method.

C. Nuclear initial conditions

For the purpose of determining the nuclear initial conditions, the electronic state $|\varphi(0)\rangle = |E_0\rangle$ ($H_{\mathrm{elec}}|E_0\rangle = E_0|E_0\rangle$) is assumed to be well described by a single Slater determinant for which [recall Eq. (9)]

$$\langle\varphi(0)|c^\dagger_{\epsilon,s}c_{\epsilon',s}|\varphi(0)\rangle = \delta_{\epsilon,\epsilon'}f(\epsilon, s), \tag{14}$$

where $f(\epsilon, s)$ is the initial electronic distribution (ground or excited) that takes values 0 or 1 depending on the initial occupation of each level with energy ϵ and spin s. The starting optimal (minimum energy) geometry is obtained by minimizing the total energy of the chain by an iterative self-consistent procedure. Specifically, the energy gradient of the oligomer is given by

$$\begin{aligned} \frac{\partial E(\boldsymbol{u})}{\partial u_m} &= \langle\varphi(0)|\frac{\partial H}{\partial u_m}|\varphi(0)\rangle = 2\alpha\mathrm{Re}\{\rho_{m,m-1} - \rho_{m,m+1}\} \\ &\quad + K(2u_m - u_{m-1} - u_{m+1}). \end{aligned} \tag{15}$$

At the optimal geometry, for which the gradient equals zero, the $m = 2, \ldots, N-1$ displacement satisfies

$$u_m = \frac{1}{2}(u_{m+1} + u_{m-1}) - \frac{\alpha}{K}\mathrm{Re}\{\rho_{m,m-1} - \rho_{m,m+1}\}. \tag{16}$$

Equation (16) is solved iteratively with the additional constraint that the boundaries of the chain are clamped ($u_1 = u_N = 0$).

Subsequently, a harmonic approximation to the nuclear ground-state wavefunction is obtained by performing a normal mode analysis around the equilibrium minimum energy geometry $\boldsymbol{u}^0 = (u^0_1, \ldots, u^0_N)$ in the (ground or excited) initial electronic state $|E_0\rangle$. For this, the Hamiltonian is expressed as a sum of the static equilibrium configuration H_0 and a dynamical part due to deviations from equilibrium

$$H = H_0 + H'_{\pi-\mathrm{ph}} + H'_{\mathrm{ph}}, \tag{17}$$

where

$$H'_{\pi-\mathrm{ph}} = \alpha\sum_{n=1,s}^{N-1}(\eta_{n+1} - \eta_n)\left(c^\dagger_{n+1,s}c_{n,s} + c^\dagger_{n,s}c_{n+1,s}\right)$$

$$\begin{aligned} H'_{\mathrm{ph}} &= \sum_{n=1}^{N}\frac{p_n^2}{2M} \\ &\quad + \frac{K}{2}\sum_{n=1}^{N-1}\left[2\left(u^0_{n+1} - u^0_n\right)(\eta_{n+1} - \eta_n) + (\eta_{n+1} - \eta_n)^2\right], \end{aligned}$$

with η_n being the displacement of the nth monomer from its equilibrium position $\eta_n = u_n - u^0_n$. In order to get the potential energy of the chain around the equilibrium geometry, the quantity $H'_{\pi-\mathrm{ph}}$ is considered as a perturbation to H_0

(Refs. 40 and 41) and we have to second order that,

$$E(\boldsymbol{\eta}) = E_0 + \langle E_0|H'_{\pi-\mathrm{ph}}|E_0\rangle + \sum_{i\neq 0}\frac{|\langle\varphi_i|H'_{\pi-\mathrm{ph}}|E_0\rangle|^2}{E_0 - E_i} + \frac{K}{2}\sum_{n=1}^{N-1}\left[2\left(u^0_{n+1} - u^0_n\right)(\eta_{n+1} - \eta_n) + (\eta_{n+1} - \eta_n)^2\right], \tag{18}$$

where we have traced over the electronic coordinates and assumed that the system is initially prepared in the electronic state $|E_0\rangle$ with energy E_0. Here $\{|\varphi_i\rangle, E_i\}$ are the eigenstates and eigenvalues of the $\mathcal{N}$-particle electronic Hamiltonian in the optimal geometry H_0.

A harmonic version of Eq. (18) is obtained by making a Taylor expansion of the potential around the equilibrium position and keeping terms up to second order in the nuclear displacements. We note that second-order perturbation in $H_{\pi-\mathrm{ph}}$ is consistent with the harmonic approximation. The effective harmonic phonon potential energy thus obtained is

$$E^{\mathrm{harm}}(\boldsymbol{\eta}) = E_0 + \frac{1}{2}\sum_{n,m=2}^{N-1}\eta_n f_{n,m}\eta_m. \tag{19a}$$

Here $f_{n,m}$ is the Hessian of the potential energy given by

$$f_{n,m} = \left.\frac{\partial^2 E}{\partial\eta_n\,\partial\eta_m}\right|_{\boldsymbol{\eta}=\mathbf{0}} = V_{nm} + K(2\delta_{n,m} - \delta_{n,m+1} - \delta_{n,m-1}), \tag{19b}$$

where

$$V_{nm} = 2\alpha^2\sum_{\epsilon,\epsilon',s}\frac{f(\epsilon',s)(1-f(\epsilon,s))}{\epsilon'-\epsilon}V^m(\epsilon,\epsilon')V^n(\epsilon,\epsilon'),$$

$$V^n(\epsilon,\epsilon') = \langle\epsilon|n\rangle\left(\langle n-1|\epsilon'\rangle - \langle n+1|\epsilon'\rangle\right) + \langle n|\epsilon'\rangle\left(\langle\epsilon|n-1\rangle - \langle\epsilon|n+1\rangle\right). \tag{19c}$$

In deriving Eq. (19), we have imposed clamped ends on the polymer chain ($\eta_1 = \eta_N = 0$). The orbitals $|\epsilon\rangle$ and their associated energies ϵ are obtained by diagonalizing the electronic Hamiltonian at the equilibrium geometry. The normal mode coordinates and frequencies are then computed by the standard analysis.[42] The eigenvectors of f_{nm} provide the normal mode coordinates $Q_j(\boldsymbol{\eta})$ and the associated eigenvalues λ_j the normal mode frequencies $\omega_j = \sqrt{\lambda_j/M}$.

A phase-space like description of the resulting nuclear quantum state is obtained by constructing the associated nuclear Wigner phase-space distribution function $\rho_{\mathrm{W}}(\boldsymbol{u},\boldsymbol{p})$. In the normal mode coordinates, $\rho_{\mathrm{W}}(\boldsymbol{u},\boldsymbol{p})$ is just the product of the Wigner distributions associated with each vibrational mode

$$\rho_{\mathrm{W}}(\boldsymbol{u},\boldsymbol{p}) = \prod_{j=1}^{N-2}\rho_j(Q_j(\boldsymbol{u}), P_j(\boldsymbol{p})), \tag{20}$$

where $Q_j(\boldsymbol{u})$ is the normal mode coordinate of the jth mode and $P_j(\boldsymbol{p})$ is its conjugate momentum. We take the chain to be initially prepared in its ground vibrational state so that[39]

$$\rho_j(Q_j, P_j) = \frac{1}{\pi\hbar}\exp\left(-M\omega_j Q_j^2/\hbar\right)\exp\left(-P_j^2/\hbar\omega_j M\right) \tag{21}$$

for $j = 1, \ldots, N-2$. The $2N-4$ dimensional phase-space distribution in Eq. (20) completely characterizes the initial quantum state of the nuclei.

The ensemble of lattice initial conditions, $\{\boldsymbol{u}^i(0), \boldsymbol{p}^i(0)\}$, for the quantum-classical dynamics is obtained from a Monte Carlo sampling of the nuclear Wigner phase-space distribution of Eq. (20). The average classical energy of the resulting ensemble coincides numerically with the zero-point energy of the lattice. The associated initial values for the orbitals $\{|\epsilon^i\rangle\}$ are obtained by diagonalizing H_{elec} in the initial lattice geometries $\{\boldsymbol{u}^i\}$. Each initial condition i, together with the equations of motion, defines a quantum-classical trajectory $(\boldsymbol{u}^i(0), \boldsymbol{p}^i(0), |\varphi^i(0)\rangle) \to (\boldsymbol{u}^i(t), \boldsymbol{p}^i(t), |\varphi^i(t)\rangle)$ and the set is employed to obtain ensemble averages. Results shown here are averages over 10000 trajectories.

III. RESULTS AND DISCUSSION

Throughout, we study neutral oligomers with an even number N of CH units. In the ground state, the geometry of the chain consists of a centrosymmetric structure with perfect alternation of double and single bonds. The single-particle spectrum of chains of different length is shown in Fig. 2. It has a total width of $4t_0 = 10$ eV and consists of $N/2$ fully occupied valence states and $N/2$ initially empty conduction states. Note how the single-particle spectrum gets more dense as the number of CH units is increased.

As a measure of electronic coherence and decoherence we follow the dynamics of the molecular polarization, defined by $\langle\hat{\mu}(t)\rangle = \langle\Psi(t)|\hat{\mu}|\Psi(t)\rangle$, where $|\Psi\rangle$ denotes the vibronic

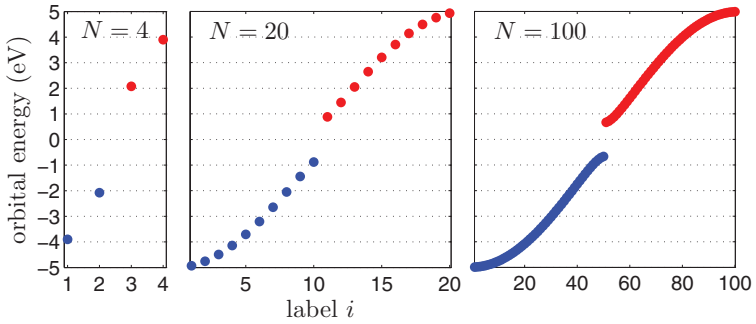

FIG. 2. Orbital energies for optimized PA chains of varying length. The valence (conduction) orbital energies are plotted in blue (red).

wavefunction and where the dipole operator $\hat{\mu} = \hat{\mu}_e + \hat{\mu}_N$ has both an electronic $\hat{\mu}_e$ and a nuclear $\hat{\mu}_N$ component. Doing so provides a measure of electronic coherence that is directly related to measurables.

It is advantageous to connect this discussion of decoherence based on the polarization to standard measurements of decoherence.[8,43] The density matrix associated with a general entangled vibronic Born-Oppenheimer state of the form $|\Psi(t)\rangle = \sum_n e^{-iE_n t/\hbar}|\varphi_n\rangle|\chi_n(t)\rangle$ is given by

$$|\Psi(t)\rangle\langle\Psi(t)| = \sum_{nm} e^{-i\omega_{nm}t}|\varphi_n\rangle|\chi_n(t)\rangle\langle\varphi_m|\langle\chi_m(t)|, \quad (22)$$

where $|\varphi_n\rangle$ are the electronic eigenstates $[H_{\text{elec}}|\varphi_n\rangle = E_n|\varphi_n\rangle]$, $|\chi_n(t)\rangle$ the nuclear wavepacket associated with each electronic level and $\omega_{nm} = (E_n - E_m)/\hbar$. If our interest is in the electronic degrees of freedom only, then the vibrations are regarded as the environment. Since we have no interest in the behavior of the environment we trace over these modes to give the density matrix of the electronic subsystem,

$$\rho_e(t) = \sum_{nm} e^{-i\omega_{nm}t}\langle\chi_m(t)|\chi_n(t)\rangle|\varphi_n\rangle\langle\varphi_m|. \quad (23)$$

Note that the off-diagonal elements of $\rho_e(t)$ are determined by the nuclear overlaps $S_{nm}(t) = \langle\chi_m(t)|\chi_n(t)\rangle$ and the loss of such coherences in $\rho_e(t)$ is a result of the evolution of the $S_{nm}(t)$ due to the vibronic dynamics. Standard measures of decoherence capture precisely this. For example, the purity of such entangled vibronic state is given by

$$\text{Tr}(\rho_e^2(t)) = \sum_{nm} |\langle\chi_m(t)|\chi_n(t)\rangle|^2 \quad (24)$$

and decays with the overlaps of the nuclear wavepackets in the different electronic surfaces.

The polarization is also a useful measure of decoherence because its magnitude also depends on the $S_{nm}(t)$. To see this consider the expression for the polarization for the entangled state in Eq. (22),

$$\langle\hat{\mu}(t)\rangle = \sum_n \langle\chi_n(t)|\mu_N|\chi_n(t)\rangle + \sum_{n,m} e^{-i\omega_{nm}t}\mu_e^{mn}\langle\chi_m(t)|\chi_n(t)\rangle, \quad (25)$$

where $\mu_e^{mn} = \langle\varphi_m|\hat{\mu}_e|\varphi_n\rangle$. Suppose that the PA chain is prepared in a spatially symmetric state where the initial nuclear state is invariant under reflection, i.e., $\rho_W(-\boldsymbol{u}, -\boldsymbol{p}) = \rho_W(\boldsymbol{u}, \boldsymbol{p})$. Since there is no symmetry breaking term in the Hamiltonian, this initial symmetry is maintained throughout the dynamics[44] and $\langle\chi_n|\mu_N|\chi_n\rangle = \mu_e^{nn} = 0$ for all n. Under such conditions, the polarization

$$\langle\hat{\mu}(t)\rangle = \sum_{n,m\neq n} e^{-i\omega_{nm}t}\mu_e^{mn}\langle\chi_m(t)|\chi_n(t)\rangle \quad (26)$$

is a direct measure of the off-diagonal matrix elements of the electronic reduced density matrix [cf. Eq. (23)]. Its evolution and decay directly offers information about the decoherence dynamics.

Note that in writing Eq. (26) we have adopted the Franck-Condon approximation where the electronic transition dipole surfaces $\mu_e^{mn}(\boldsymbol{u})$ are assumed to depend weakly on the nuclear displacements. However even when this approximation is not valid, a decay in $\langle\hat{\mu}(t)\rangle$ will still signal a decay in the nuclear overlaps, albeit modulated by the dependence of the electronic transition dipoles on the nuclear coordinates.

Thus, both $\text{Tr}(\rho_e^2(t))$ and $\langle\hat{\mu}(t)\rangle$ are useful measures of decoherence and both decay with the overlaps of the nuclear wavepackets in different electronic states. The advantage of the polarization over the purity is that it is a physically accessible observable. Its limitation, however, is that $\langle\hat{\mu}(t)\rangle$ only signals coherences for which $\mu_e^{mn} \neq 0$. So, for instance, coherences between eigenstates of the same parity are absent in the polarization even when they would contribute to the purity.

In the quantum-classical picture of the dynamics, the polarization is computed as an average of the polarizations recorded for each of the $\mathcal{M}$ individual trajectories in the ensemble,

$$\langle\hat{\mu}(t)\rangle = \frac{|e|}{\mathcal{M}}\sum_{i=1}^{\mathcal{M}}\sum_{n=1}^{N} x_n^i(t)\left(1 - \rho_{n,n}^i\right), \quad (27)$$

where $x_n^i(t) = (na + u_n^i(t))$ is the position of site n at time t in the ith trajectory and e is the electron charge. The first term in Eq. (27) comes from the dipole due to the nuclei, while the second one quantifies the electronic contributions.

There are two possible effects that can lead to a decay of the electronic coherences (recall Fig. 1): anharmonicities in the potential and population transfer into other electronic states. More precisely, if there is no population transfer into other states, and the electronic potential energy surfaces are bounded, then anharmonicities in the electronic potential energy surfaces can lead to a spread of the nuclear wavepackets during evolution and thus to a decay of the nuclear overlap integral $S_{ij} = \langle\chi_j(t)|\chi_i(t)\rangle$ (wavepacket evolution in purely harmonic potentials lead to periodic recurrences in S_{ij} and thus cannot lead to decoherence). Alternatively, population transfer into other electronic states can lead to decoherence by transferring population to states for which only poor overlaps of the nuclear wavepackets are possible with the states already involved in the superposition. This poor overlap arises because different electronic potential energy surfaces typically have substantially different gradients and position of their minima in conformational space, leading to diverging evolution of the nuclear wavepackets in the excited state manifold.

It should be noted that, traditionally, studies of the decoherence of a superposition state would not typically include loss of population from the state, which would be regarded as a relaxation, rather than decoherence, process. However, this distinction is meaningful when energy transfer and decoherence time scales are substantially different, the latter occurring on much shorter time scales than the former. Here, however, as shown below, population transfer between states occur rather quickly, making this subdivision less meaningful, and making such contributions quite significant in the time evolution of $\langle\hat{\mu}(t)\rangle$ and the purity. Here then, we use the term "decoherence" to relate to any process that causes loss of the coherence of $\langle\hat{\mu}(t)\rangle$.

Below we discuss several examples of decoherence dynamics in PA chains. The interpretation of the results will

be done in a wavepacket language and with the wavepacket picture of Fig. 1 in mind, even though the computations are performed in a mixed quantum-classical setting. Such wavepacket evolution is captured by the quantum-classical dynamics through the time dependence of the orbital energies and populations in the ensemble of trajectories.

A. Decoherence between the ground and first excited state for chains of different lengths

Consider first the decoherence dynamics of PA chains initially in a separable superposition state of the form,

$$|\Psi(0)\rangle = \frac{1}{\sqrt{2}}(|\varphi_0\rangle + |\varphi_1\rangle) \otimes |\chi_{00}\rangle, \tag{28}$$

where $|\varphi_0\rangle$ is the ground electronic state, $|\varphi_1\rangle$ is the first excited state (obtained by promoting an electron from the HOMO to the LUMO) and $|\chi_{00}\rangle$ is the ground state nuclear wavefunction in the ground electronic surface. Physically, such a superposition can be created by instantaneous (delta pulse) excitation of the relaxed ground state chain. Figure 3 shows $\langle\hat{\mu}(t)\rangle$ for chains with varying number of CH units (N). The high frequency oscillations in $\langle\hat{\mu}(t)\rangle$ are due to the difference in energy between the two states involved in the superposition (in this case the energy gap). The remaining time dependence arises from the wavepacket evolution in the excited state potential energy surface. For the four site chain, the polarization displays a fast initial decay with recurrences every ∼30 fs. These recurrences arise from the time dependence of the overlap of the nuclear wavefunctions in the ground and excited electronic states [see Eq. (26)], and signal the oscillatory motion of the nuclear wavepacket in the excited state potential. Between consecutive recurrences the amplitude of the polarization diminishes and eventually dies out, yielding a

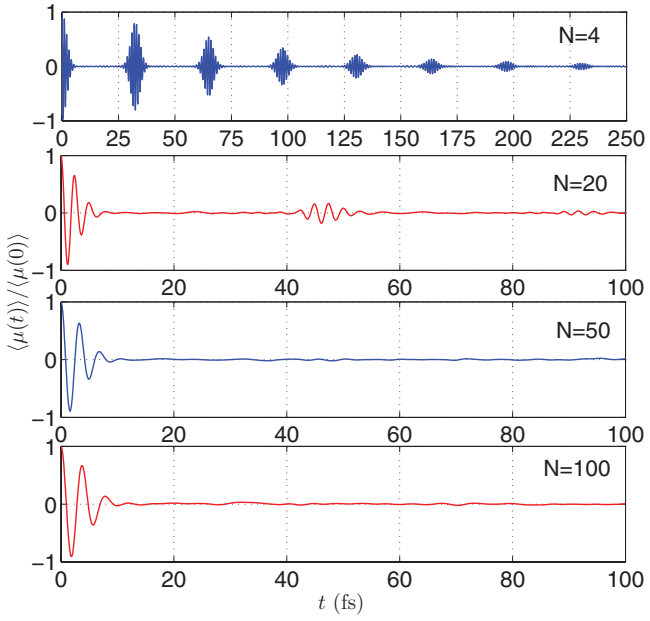

FIG. 3. Electronic decoherence dynamics in chains of different lengths N. The figure shows the evolution and decay of the chain polarization when the system is initially prepared in a superposition between the ground and first excited state of the form in Eq. (28).

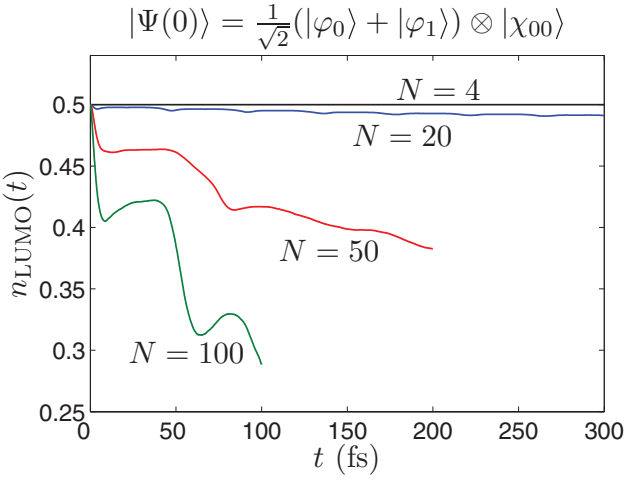

FIG. 4. Population of the LUMO orbital during the decoherence dynamics of a N-site SSH chain with the initial conditions of Eq. (28).

decoherence time scale of ∼250 fs for $N = 4$. For $N = 20$ we observe only two of these recurrences, occurring every ∼46 fs to yield a decoherence time of ∼100 fs. For longer oligomers ($N = 50$ and $N = 100$) no recurrences are observed and the decoherence occurs in less than 10 fs.

Additional insights into the decoherence dynamics can be extracted by considering the evolution of the population of the LUMO of the chain (Fig. 4). If the main decoherence mechanism is the anharmonic evolution of the nuclear wavepacket in the first excited state potential energy surface, then one should expect little population exchange with other levels of the chain. As shown in Fig. 4 for $N = 4$ and $N = 20$ an almost negligible amount of population is transferred to other electronic states, suggesting that anharmonicities are the main source of decoherence. By contrast, for long chains ($N = 50$ and $N = 100$) the electronic spectrum is so dense that a substantial amount of population is transferred from the initially populated LUMO to other electronic states. This suggests that both anharmonicities and population decay to other electronic states contribute to the decoherence, leading to an evolution with no apparent recurrences.

B. Decoherence of superpositions between excited states

We now investigate how the decoherence dynamics changes when the initial superposition is between two excited states rather than between an excited and ground electronic state. For this we consider the two classes of model initial superpositions schematically represented in Fig. 5. In the first class, the initial state is of the form

$$|\Psi(0)\rangle = \frac{1}{\sqrt{2}}(|\phi_i\rangle + |\phi_{i+1}\rangle) \otimes |\chi_{00}\rangle, \tag{29}$$

where $|\phi_i\rangle = c^\dagger_{i,s} c_{N/2,s} |\varphi_0\rangle$ ($i \in \{N/2+1, \ldots, N\}$) is an electronically excited state obtained by promoting an electron from the HOMO to the ith orbital level of the ground state $|\varphi_0\rangle$. In this superposition the initial nuclear state is taken to be the ground vibrational state in the ground electronic surface, $|\chi_{00}\rangle$. Physically, such a superposition will arise via

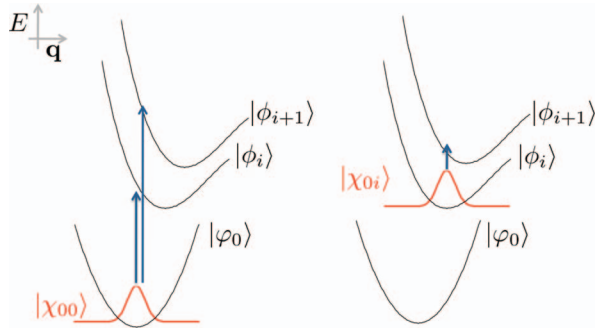

FIG. 5. Schematic of the process used to create the superpositions in Eq. (29) (left panel) and Eq. (30) (right panel).

instantaneous excitation of the ground vibronic state into states $|\phi_i\rangle$ and $|\phi_{i+1}\rangle$, as depicted in the left panel of Fig. 5. By contrast, in the second class of superpositions the nuclei are taken to be initially prepared in the ground state distribution of the *excited* electronic state $|\phi_i\rangle$, so that

$$|\Psi(0)\rangle = \frac{1}{\sqrt{2}}(|\phi_i\rangle + |\phi_{i+1}\rangle) \otimes |\chi_{0i}\rangle. \tag{30}$$

The wavefunction $|\chi_{0i}\rangle$ is obtained by finding the optimal geometry of the electronically excited state and then performing a normal mode analysis around this geometry, as discussed in Sec. II C. Physically such a superposition will arise from instantaneous excitation of a chain vibrationally relaxed in state $|\phi_i\rangle$ to state $|\phi_{i+1}\rangle$, as represented in the right panel of Fig. 5.

1. The case of a 20-site chain

Consider first the case of a chain with 20 CH units. The left panels in Fig. 6 show the time dependence of the polarization when the system is initially prepared in the superposition in Eq. (29) for different i's. The figure shows that the decoherence dynamics can change substantially depending on the pair of states that are selected to form the superposition. It is even possible to find superpositions for which the coherences are unusually long lived. For example, for $i = 15$ the electronic coherences survive for ~200 fs, a time scale that is comparable to the coherence lifetime observed in photosynthetic systems.

Additional insights into the decoherence mechanisms are provided by the shape of $\langle\hat{\mu}(t)\rangle$ and by the dynamics of population in the excited orbitals (Fig. 7). The polarization indicates that for $i = 11$ there is vibronic evolution in the excited states that leads to a decay and to the recurrence of the nuclear overlap integrals determining $\langle\hat{\mu}(t)\rangle$. By contrast, for $i = 19$ this motion is not apparent in $\langle\hat{\mu}(t)\rangle$ which shows a decay in ~60 fs with no apparent additional structure. The population dynamics (Fig. 7, upper panel) complements this picture by showing that for $i = 11$ a negligible amount of population decays to other levels, while for $i = 19$ the transfer of population to other levels is substantial. These observations suggest that for $i = 11$ the main mechanism for decoherence is due to anharmonicities in the excited state potential energy surfaces, while for $i = 19$ the main decoherence mechanism is due to population transfer to other electronically excited states for which only poor nuclear overlaps are possible. The case of $i = 15$ is discussed below.

As an additional test of these observations consider the dynamics of superpositions between the same set of levels but starting from Eq. (30), that uses a different initial nuclear state. The results are shown in the right panel of Fig. 6. As can be seen, for $i = 11$ changing the initial nuclear state triples the coherence lifetime of the superposition, with three visible recurrences instead of one. Since for this superposition there is negligible amount of population being transferred to other electronic states (see Fig. 7), the data confirm

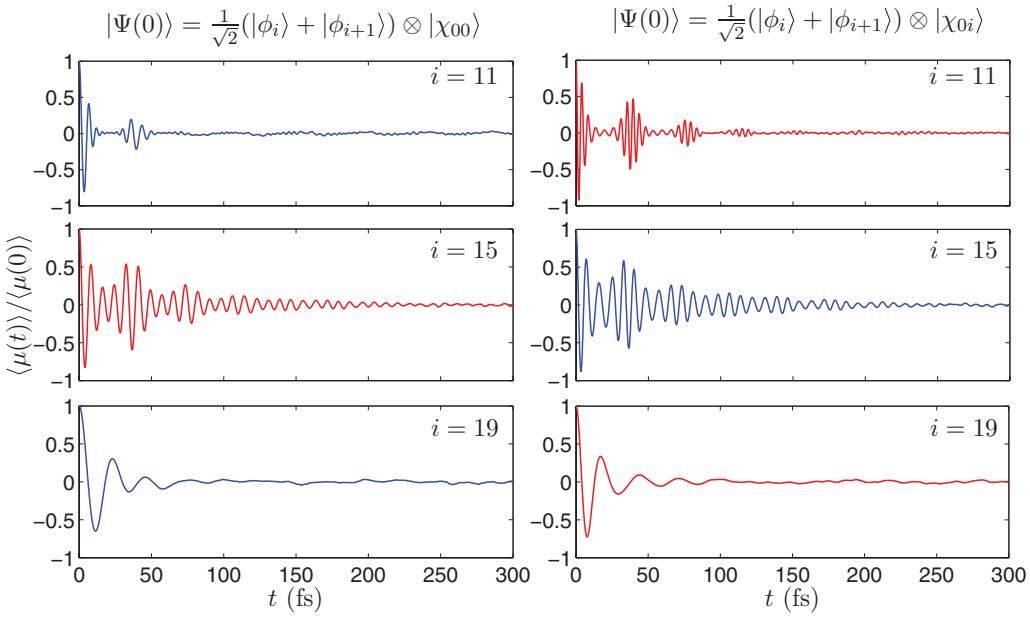

FIG. 6. Electronic decoherence dynamics in a 20 site chain for different initial superposition between excited states. The panels show the dynamics and decay of the chain polarization starting from a superposition of the form in Eq. (29) (left panels) or Eq. (30) (right panels).

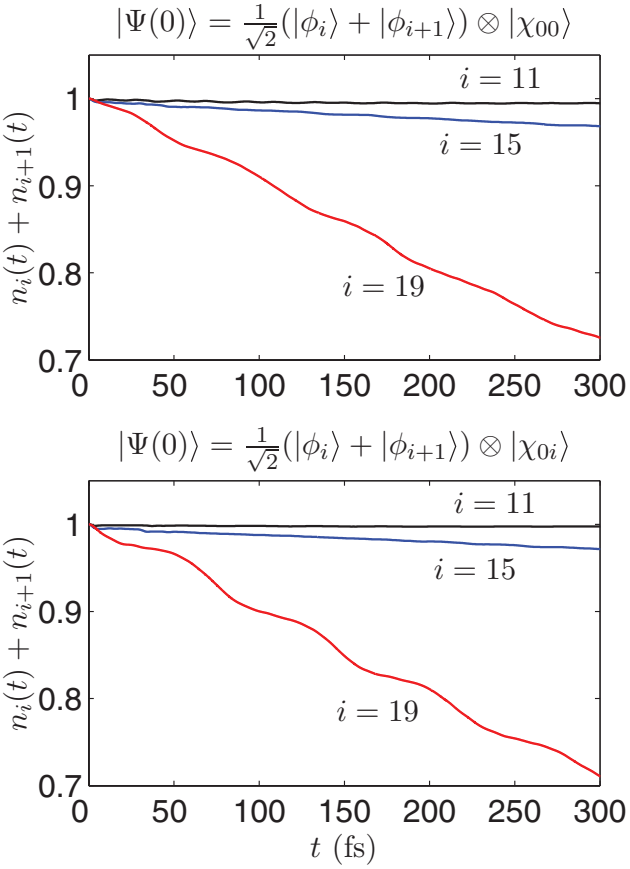

FIG. 7. Combined population of the ith and $(i + 1)$th orbitals during the decoherence dynamics of a 20-site SSH chain starting from the initial superpositions depicted in Fig. 5.

that anharmonicities in the potential energy surfaces of the excited states are the main source of the decoherence in this case. By contrast, for $i = 19$ changing the nature of the initial nuclear state has little effect on the decoherence dynamics, suggesting that the main decoherence mechanism in this case is due to population transfer to other electronic states, as seen in Fig. 7.

The case for $i = 15$ where long coherences are observed is different. For this superposition, little population is transferred to other electronic states and a change in the initial nuclear state has little effect on the decoherence dynamics. This suggests that this superposition is protected from decoherence both by the fact that the density of states is such that the two states involved in the superpositions are weakly coupled to other electronic states, and because the sampled potential energy surfaces are less anharmonic than in the other cases considered.

2. The case of a 100-site chain

For larger systems the situation is qualitatively different. Figure 8 shows the dynamics of the polarization for chains initially in a superposition state of the form in Eqs. (29) and (30) for different i. Figure 9 shows the associated change in population of the ith and $(i + 1)$th orbitals. The electronic spectrum is so dense that upon evolution significant population is transferred to other electronic states. Irrespective of the type of superpositions considered or the initial nuclear state coherence decay in this chain is extremely fast, of the order of 50 fs. The electronic spectrum in this system is simply too dense to maintain electronic coherence. In $\langle\mu(t)\rangle$, however, for $i = 51$ population loss is less than in the other two cases, consistent with the fact that some oscillatory character is visible for $i = 51$ in Fig. 8.

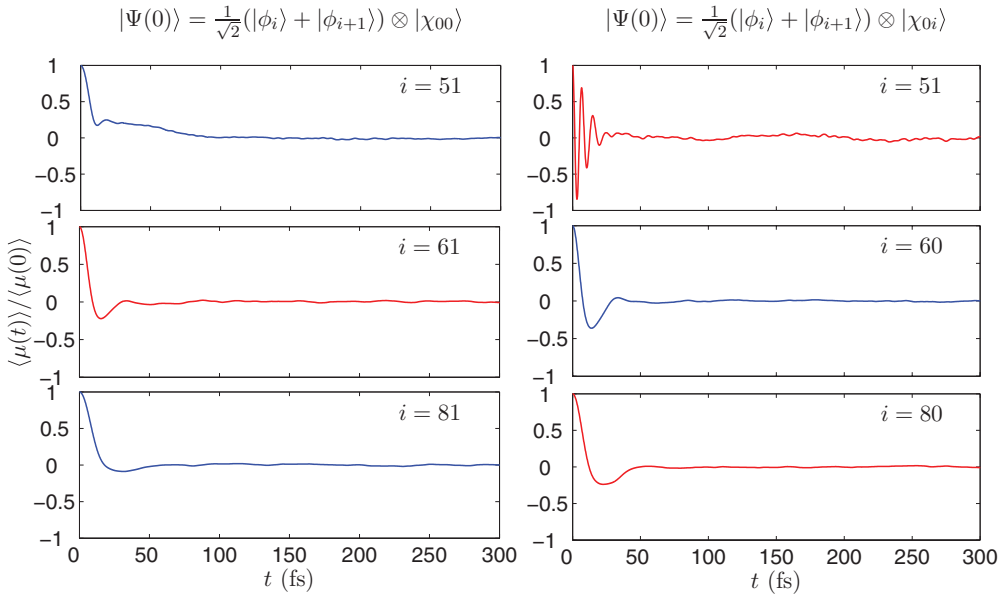

FIG. 8. Electronic decoherence dynamics in a 100 site chain for different initial superposition states. The panels show the dynamics and decay of the chain polarization starting from a superposition of the form in Eq. (29) (left panels) or Eq. (30) (right panels).

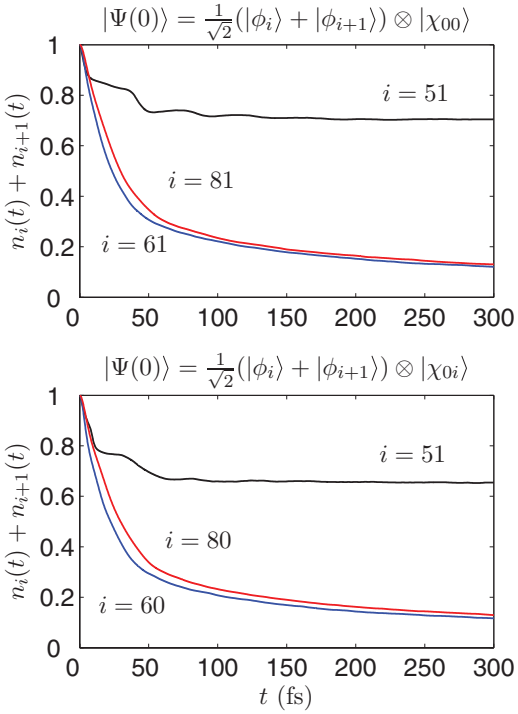

FIG. 9. Combined population of the ith and $(i + 1)$th orbitals during the decoherence dynamics of a 100-site SSH chain starting from the initial superpositions described in Fig. 5.

IV. CONCLUSIONS

In this paper, we have presented numerical simulations of the electronic coherence dynamics of PA oligomers of varying length in which the evolution of both electrons and nuclei are followed explicitly in a mixed quantum-classical approximation. We investigated the decoherence of superpositions, as manifest in the dynamics of the polarization, between the ground and excited and between pairs of excited states. Decoherence is caused by the decay of the overlap of the nuclear wavepackets associated with all electronic states involved in the superposition. Two basic mechanisms for such decay were identified: population transfer into other electronic states where only poor overlaps are possible, and vibronic evolution in anharmonic potential energy surfaces that lead to wavepacket spread.

The simulations indicate that for long chains (e.g., $N = 100$) the electronic spectrum is so dense that decoherence is dominated by population decay into other states. In this case, no recurrences are observed in the polarization and the decoherence occurs in tens of femtoseconds. Further, the decoherence dynamics was found to be largely independent of the type of initial superposition that is subject to the decoherence. By contrast, for shorter chains (e.g., $N = 20$) the simulations indicate that the decoherence dynamics depends strongly on the initial vibronic state. We identified superpositions for which anharmonicities were the main source of decoherence and superpositions for which population transfer to other electronic states was determinant. Interestingly, we also observed a superposition state between excited states with coherence properties that are long lived, for ~200 fs. Such a superposition was found to be long lived because it is spectrally isolated from other electronic states and because the vibronic dynamics leads to a relatively slow spread of the nuclear wavepackets.

ACKNOWLEDGMENTS

This work was supported by the National Sciences and Engineering Research Council of Canada, and by a grant from the U.S. Air Force Office of Scientific Research (USAFOSR) under Contract No. FA9550-10-1-0260. I.F. thanks Professor Mark A. Ratner and Professor George C. Schatz for their support during the preparation of this manuscript.

[1] I. Franco, M. Shapiro, and P. Brumer, J. Chem. Phys. **128**, 244905 (2008).
[2] B. G. Levine and T. J. Martínez, Annu. Rev. Phys. Chem. **58**, 613 (2007).
[3] Y.-C. Cheng and G. R. Fleming, Annu. Rev. Phys. Chem. **60**, 241 (2009).
[4] H. P. Breuer and F. Petruccione, *The Theory of Open Quantum Systems* (Oxford University Press, New York, 2002).
[5] S. H. Choi, C. Risko, M. C. R. Delgado, B. Kim, J.-L. Brédas, and C. D. Frisbie, J. Am. Chem. Soc. **132**, 4358 (2010).
[6] R. Kapral, Annu. Rev. Phys. Chem. **57**, 129 (2006).
[7] J. E. Subotnik and N. Shenvi, J. Chem. Phys. **134**, 244114 (2011).
[8] M. Shapiro and P. Brumer, *Quantum Control of Molecular Processes* (Wiley-VCH, Weinheim, 2012).
[9] M. Nielsen and I. Chuang, *Quantum Computation and Quantum Information* (Cambridge University Press, 2000).
[10] H. Hwang and P. J. Rossky, J. Phys. Chem. B **108**, 6723 (2004).
[11] H. Kamisaka, S. V. Kilina, K. Yamashita, and O. V. Prezhdo, Nano Lett. **6**, 2295 (2006).
[12] B. F. Habenicht, H. Kamisaka, K. Yamashita, and O. V. Prezhdo, Nano Lett. **7**, 3260 (2007).
[13] G. S. Engel, T. R. Calhoun, E. L. Read, T.-K. Ahn, T. Mancal, Y.-C. Cheng, R. E. Blankenship, and G. R. Fleming, Nature (London) **446**, 782 (2007).
[14] H. Lee, Y.-C. Cheng, and G. R. Fleming, Science **316**, 1462 (2007).
[15] E. Collini, C. Y. Wong, K. E. Wilk, P. M.G. Curmi, P. Brumer, and G. D. Scholes, Nature (London) **463**, 644 (2010).
[16] M. Mohseni, P. Rebentrost, S. Lloyd, and A. Aspuru-Guzik, J. Chem. Phys. **129**, 174106 (2008).
[17] S. Lloyd, Nat. Phys. **5**, 164 (2009).
[18] A. Ishizaki and G. R. Fleming, Proc. Natl. Acad. Sci. U.S.A. **106**, 17255 (2009).
[19] J. S. Briggs and A. Eisfeld, Phys. Rev. E **83**, 051911 (2011).
[20] G. Katz, D. Gelman, M. A. Ratner, and R. Kosloff, J. Chem. Phys. **129**, 034108 (2008).
[21] N. Renaud, M. A. Ratner, and V. Mujica, J. Chem. Phys. **135**, 075102 (2011).
[22] A. Ishizaki and G. R. Fleming, J. Chem. Phys. **130**, 234111 (2009).
[23] A. Kelly and Y. M. Rhee, J. Phys. Chem. Lett. **2**, 808 (2011).
[24] L. Pachon and P. Brumer, J. Phys. Chem. Lett. **2**, 2728 (2011).
[25] L. Pachon and P. Brumer, "Computational methodologies and physical insights into electronic energy transfer in photosynthetic light-harvesting complexes," Phys. Chem. Chem. Phys. (submitted), online at http://arxiv.org/pdf/1203.3978v1.pdf.
[26] P. Huo and D. Coker, J. Phys. Chem. Lett. **2**, 825 (2011).
[27] F. Sterpone, R. Martinazzo, A. N. Panda, and I. Burghardt, Z. Phys. Chem. **225**, 541 (2011).
[28] A. J. Heeger, S. Kivelson, J. R. Schrieffer, and W. P. Su, Rev. Mod. Phys. **60**, 781 (1988).
[29] T. Teramoto, Z. Wang, V. M. Kobryanskii, T. Taneichi, and T. Kobayashi, Phys. Rev. B **79**, 033202 (2009).
[30] S. Adachi, V. M. Kobryanskii, and T. Kobayashi, Phys. Rev. Lett. **89**, 027401 (2002).
[31] S. Tretiak, A. Saxena, R. L. Martin, and A. R. Bishop, Proc. Natl. Acad. Sci. U.S.A. **100**, 2185 (2003).
[32] L. Stella, R. P. Miranda, A. P. Horsfield, and A. J. Fisher, J. Chem. Phys. **134**, 194105 (2011).
[33] H. Ness and A. J. Fisher, Phys. Rev. Lett. **83**, 452 (1999).
[34] J. C. Tully, in *Classical and Quantum Dynamics in Condensed Phase Simulations*, edited by B. Berne, G. Ciccotti, and D. F. Coker (World Scientific, Singapore, 1998), pp. 700–720.

[35]H. W. Streitwolf, Phys. Rev. B **58**, 14356 (1998).
[36]A. Johansson and S. Stafström, Phys. Rev. B **65**, 045207 (2002).
[37]I. Franco, M. Shapiro, and P. Brumer, J. Chem. Phys. **128**, 244906 (2008).
[38]I. Franco, M. Shapiro, and P. Brumer, Phys. Rev. Lett. **99**, 126802 (2007).
[39]M. Hillery, R. F. O'Connell, M. O. Scully, and E. P. Wigner, Phys. Rep. **106**, 121 (1984).
[40]K. A. Chao and Y. Wang, J. Phys. C **18**, L1127 (1985).
[41]E. J. Mele and M. J. Rice, Phys. Rev. Lett. **45**, 926 (1980).
[42]E. B. Wilson, J. C. Decius, and P. C. Cross, *Molecular Vibrations* (Dover, New York, 1980).
[43]M. Schlosshauer, *Decoherence and the Quantum-to-Classical Transition* (Springer, New York, 2008).
[44]I. Franco and P. Brumer, J. Phys. B **41**, 074003 (2008).